PACS numbers: 42.55.Lt; 42.65.Dr
DOI: 10.1070/QE2002v032n05ABEH002218

Spectrum of an anti-Stokes Raman ion laser in Λ-schemes with various level parameters

S.A. Babin, S.I. Kablukov, S.M. Kobtsev, V.V. Potapov, D.V. Churkin

***Abstract*. The dependence of the Raman-laser output power in a standing-wave mode on the pump frequency located near the resonance with ionic levels is studied. The emission spectra in two Λ-schemes of Ar II with different lifetimes of the final levels are compared. In the scheme with a long-lived final state, a sharp peak with an amplitude exceeding the amplitude of a broad contour by a factor of 1.5–2 is observed at the exact resonance, whereas no spectral features are observed near the resonance in the scheme with a short-lived final level. The effect is analysed within the framework of a model taking into account the Coulomb scattering of ions. It is shown that the peak forms due to a difference in the broadening of the Bennett structures in the population distribution of the operating levels over velocities. In the second Λ-scheme, the contribution of the final level is small in amplitude, and a sharp peak in the spectrum disappears in accordance with the predictions of the model.**

Keywords: *Raman laser, ion laser, Λ-scheme, Coulomb broadening, diffusion width.*

1. Introduction

Despite a significant progress in the field of solid-state and semiconductor lasers, argon lasers still remain the most high-power and available sources of cw tunable radiation with a significant temporal and spatial coherence in the blue, violet, and UV spectral regions. Recently, an interest in argon lasers has increased due to the possibility of using them as sources of UV radiation for fabrication of Bragg gratings in optical fibres. Such gratings are widely used in fibreoptic telecommunication systems [1].

Direct generation in the UV region on the ArIII lines is possible in the range from 275 to 379 nm. The second harmonics of strong Ar II lines are less intense but have shorter wavelengths 244 and 257 nm. One of the promising methods for obtaining short-wavelength radiation is also the generation in the resonance anti-Stokes SRS scheme on ArII lines [2, 3]. In the Λ-scheme (Fig. 1), the pump radiation at the frequency ω_p is converted into the radiation of a Raman laser at the frequency $\omega > \omega_p$. Continuous lasing in an anti-Stokes Raman laser was obtained for the first time on atomic neon transitions [4]. A Λ-scheme with the known laser lines at 1.52 and 1.15 μm was employed. A narrow nonlinear resonance was later recorded in the dependence of the Raman-laser output power on the pump frequency (in the Raman-laser tuning curve) [5]. A shallow (< 10 %) but a sharp dip with the width of the $n - l$ forbidden transition was distinctly observed against the background of a broad spectral distribution. The pump and generated waves in the Raman-laser cavity were travelling and standing waves, respectively. Such a structure appears due to the overlap of the coherences, which are induced by the standing-wave components, in the velocity distribution. This spectrum was quantitatively described in [5], and the possibility of precisely determining the relaxation rate of the forbidden transition from the resonance was also shown. More recently, the Stokes and anti-Stokes lasing was obtained on the Ne and Ar atomic lines, which are not laser lines [6, 7].

Since the lines in ion spectra have shorter wavelengths compared to the lines in atomic spectra, the Λ-scheme using Ar II makes it possible to obtain a high conversion coefficient (~ 25 % at the maximum) in the short-wavelength spectral region [2]. The relatively long-lived initial $3d\,^2P_{3/2}$ ($\tau_n \sim 30$ ns) and intermediate $4p\,^2S^0_{1/2}$ ($\tau_m \sim 10$ ns) levels were used for radiation conversion [8, 9], and the rapidly decaying final level $4s\,^2P_{3/2}$ ($\tau_l \sim 0.35$ ns) of the Λ-scheme is the lower level of usual laser lines (see the scheme in Fig. 1b). Note that the parameters of the initial $3d\,^2P_{3/2}$ level were not optimal (the population and lifetime were small). Due to the optimisation of the initial levels of Λ-schemes on ionic transitions in the argon laser plasma, the conversion efficiency reached 60 % [3] at a tuning range of ±4 GHz. As the initial levels, the $3d'\,^2G$ and $3d\,^4F$ metastable levels without radiative relaxation can also be used. However, under discharge conditions, their lifetime is limited by collisions with electrons ($\tau < 100$ ns) [10]. The plasma features of the active medium results in the appearance of new effects caused by ion–ion collisions [11], which, in particular, may lead to a significant increase in the Raman-laser output power.

One of such effects was discovered when investigating the tuning characteristics of a Raman ion laser [12]. A Λ-scheme with a comparatively long-lived final level was used (Fig. 1a). The pumping was performed by a traveling wave, and the generated wave was a standing one. A sharp peak

S.A. Babin, S.I. Kablukov, S.M. Kobtsev, V.V. Potapov, D.V. Churkin
Institute of Automatics and Electrometry, Siberian Branch, Russian Academy of Sciences, pr. Koptyuga 1, 603090 Novosibirsk, Russia; e-mail: babin@iae.nsk.su

Received 20 February, 2002
Kvantovaya Elektronika **32** (5) 455–459 (2002)
Translated by A.S. Seferov

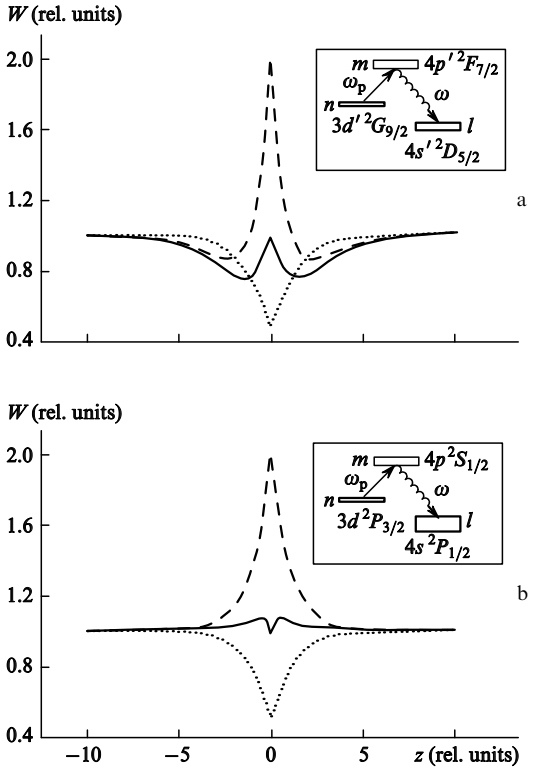

Figure 1. Spectral curves calculated from formula (1) (solid curves) for the schemes with long-lived ($q = 1.4$; a) and short-lived ($q = 0.2$; b) final levels [$q = (\Gamma_m/\Gamma_l)^{1/2}$]. Dashed and dotted lines correspond to the numerator and denominator, respectively, in formula (1). Linear absorption (amplification) is neglected. Insets present the systems of levels.

was detected in the frequency dependence of the output power, and the following relation was valid: $\Omega = (k/k_p)\Omega_p$, where $\Omega_p = \omega_p - \omega_{mn}$ and $\Omega = \omega - \omega_{ml}$ are the detunings with respect to the resonance peak, and k and k_p are the wave numbers of the generated and pump radiations. This profile of the spectral curve was unexpected, since it differed from the profile observed for atomic neon [5] in the scheme with close level parameters.

In this paper, we compare two Λ-schemes of a Raman laser. In the first scheme with a comparatively long-lived final level, the red pump radiation at 611 nm was converted into the blue light at 461 nm (see the inset in Fig. 1a). In the second scheme with a short-lived final level, the pump radiation at 648 nm was converted into the light at 458 nm (see the inset in Fig. 1b). Table 1 presents the relaxation rates Γ_n, Γ_m, and Γ_l for the levels n, m, and l and the Einstein coefficients A_{mn}, A_{ml} for the $m - n$ and $n - l$ transitions for the schemes employed. Based on the features of the influence of Coulomb collisions on the spectral characteristics of Raman lasers [12], these schemes must yield essentially different spectral dependences, which were actually observed in the experiment described below.

2. Model

The amplification of the generated wave on the $m - l$ transition is composed of the effects induced by optical pumping: the population transfer from the n level to the m level and coherent two-photon processes arising due to the polarisation ρ_{nl} at the forbidden transition. Coulomb collisions lead to the polarisation decay. The lifetime of polarisation ρ_{nl} can be estimated as $\tau_D \simeq [D(k - k_p)^2]^{-1/3} \sim 10^{-9}$ s $\ll \Gamma_m^{-1}, \Gamma_n^{-1} \leqslant \Gamma_l^{-1}$, so that coherent processes can be neglected in the analysis of the basic effects. Here, $D = v v_T^2/2$ is the diffusion coefficient in the velocity space, v is the effective rate of ion–ion collisions, and v_T is the thermal velocity.

A sharp structure at the zero detuning can be observed in the amplification contour already in the linear approximation by analysing only the population dynamics. The fields induce Bennett structures in the distribution of populations over velocities. Coulomb ion–ion collisions in the discharge plasma result in a diffusion of ions in the space of velocities; therefore, the longer the level lifetime, the larger the Bennett peak (or dip) broadening, and, its profile in the strong diffusion limit becomes exponential with the width $\Delta_{D_j} \approx k v_T (v/2\Gamma_j)^{1/2}$ ($j = m, n, l$) [13]. Therefore, changes in the distribution of the population difference over velocities at the operating $m - l$ transition of a Raman laser, which are induced by a traveling pump wave, represent the difference of the exponential contours with different widths and centered at the resonance velocity $v^* = \Omega_p/k_p$.

When the detuning with respect to the resonance is $\Omega_p > \Gamma_j, \Delta_{D_j}$, only the traveling-wave component with the same direction interacts with a pump-field-induced nonlinear structure, and $v^* = \Omega/k = \Omega_p/k_p$ in this case. At the exact resonance ($\Omega_p = 0$), the counterpropagating radiation components of the Raman laser interact with the same group of excited ions, resulting in the appearance of a sharp structure in the amplification line at $\Omega = 0$. In this case, in the scheme with a long-lived final level l, a peak against a background of a wider dip forms in the amplification line; i.e., the peak corresponding to the level m is less broadened than the peak corresponding to the level l. An opposite situation can be observed in a scheme with a short-lived final level.

In order to analyse the effect quantitatively in different schemes, we use an analytic expression derived in [12] in the following approximations: the saturation at the operating transition of a Raman laser was taken into account, the contribution of coherent effects, higher spatial harmonics, and the saturation of the pump wave absorption were neglected, and it was assumed that the diffusion width was much larger than the relaxation rates and much smaller than the Doppler width. In this case, the output power of a Raman laser has the form

$$W = C\frac{(N/\tau)f_T - 1 + (\langle P\rangle f_T/\tau)(1 + e^{-z} - B)}{1 + q + e^{-z} + q e^{-z/q} - B} \geqslant 0, \qquad (1)$$

Table 1. Level parameters.

Transitions	$\Gamma_n/10^7$ s^{-1}	$\Gamma_m/10^7$ s^{-1}	$\Gamma_l/10^7$ s^{-1}	$A_{mn}/10^7$ s^{-1}	$A_{ml}/10^7$ s^{-1}	References
$3d'^2G_{9/2} \rightarrow 4p'^2F_{7/2} \rightarrow 4s'^2D_{5/2}$	2	16	8	2	6	[8–11]
$3d^2P_{3/2} \rightarrow 4p^2S_{1/2} \rightarrow 4s^2P_{1/2}$	8	15	300	1	9	[8–11]

where

$$B = A\frac{q - 1 + qe^{-z/q} - e^{-z}}{q^2 - 1};$$

$f_T = \exp(-\Omega_p^2/k_p^2 v_T^2)$ is the Doppler factor; $z = 2|\Omega_p|/k_p \times (D/\Gamma_m)^{1/2}$ is the pump field detuning normalised to the diffusion width; $q = (\Gamma_m/\Gamma_l)^{1/2}$; $P = \pi|G_p|^2/(Dk_p^2\Gamma_m)^{1/2}$ is the dimensionless pump power; $N = 2(N_m - N_l)/(N_n - N_m)$ is the dimensionless population difference at the operating transition;

$$\tau = \frac{c|\varepsilon|^2}{8\pi}\frac{1-r}{L}\frac{kv_T}{2\hbar\omega\sqrt{\pi}|G|^2(N_n - N_m)}$$

is the dimensionless loss factor; ε is the permittivity; $1 - r$ is the loss factor; L is the cavity length; G and G_p are the Rabi frequencies; $A = A_{ml}/\Gamma_l$; $C = TS(Dk^2/\Gamma_m)^{1/2}/A_{ml}$ is the dimensional scaling factor; S is the average beam cross section; $T = 2L/c$;

$$\langle P\rangle = \frac{1}{L}\int_0^L P(x)\mathrm{d}x = P\,\frac{1 - \exp(-\alpha f_T L)}{\alpha f_T L}$$

is the pump power with allowance for an absorption-caused nonuniformity along the medium; and α is the absorption coefficient.

Two terms describing quite different phenomena can be distinguished in the numerator of formula (1). The first one $Nf_T/\tau - 1$ describes the saturated absorption (amplification) on the operating transition, and the second term is responsible for the Raman lasing under optical pumping. Note that the numerator and denominator characterise, respectively, the amplification and saturation at the $m - l$ transition. In the case of schemes with a long-lived final level ($q \gtrsim 1$), a narrow peak with a diffusion width of the upper level and a wide dip with the diffusion width of the lower level are formed. The effect exists even at equal level relaxation rates $\Gamma_m = \Gamma_l$ ($q = 1$), if a spontaneous decay is taken into consideration. For schemes with a short-lived final level ($q \to 0$), the second term is almost frequency-independent, and the numerator and denominator of (1) are canceled. The total contour can be obtained taking into account the saturated absorption (amplification) and a certain frequency-independent parameter proportional to the pump power. Hence, in this case, the tuning characteristic cannot have a sharp and intense peak unlike schemes with a long-lived final level.

Figure 1a shows that, in the scheme with a long-lived final level, a peak forms against the background of a wider dip at the center of the contour. The peak and dip widths are determined by the diffusion at the intermediate and final levels, respectively. In the scheme with a short-lived final level (Fig. 1b), the ratio of widths is inverse, and a dip with a small amplitude may be formed instead of a peak. This is caused by the fact that the contribution of a narrow contour (at the lower level in this case) is proportional to a small value $q \ll 1$.

Let us discuss the applicability of this model. Under our experimental conditions, the Doppler width is $kv_T \sim 10^{10}$ s^{-1} and the transport collision rate is $\nu \sim 10^7$ s^{-1}. For a scheme with a long-lived final level, the relaxation rates are $\Gamma_j \leqslant 10^8$ s^{-1}, the diffusion width is $\Delta_{D_j} \sim 10^9$ s^{-1}, and the approximations $\Gamma_{ij} \ll \Delta_{D_j} \ll kv_T$ and $\Gamma_{ml} \ll \tau_D^{-1}$ assumed in the theory are well satisfied. The second inequality implies that the polarisation at the forbidden transition is suppressed and coherent processes can be ignored.

For a scheme with a short-lived final level, $\Gamma_n, \Gamma_m \sim 10^8$ s^{-1}, $\Gamma_l \sim 10^9$ s^{-1}, $\Delta_{D_m} \sim 10^9$ s^{-1}, $\Delta_{D_l} \sim 10^8$ s^{-1}. Therefore, for the levels n and m, the approximation $\Gamma_j \ll \Delta_{D_j} \ll kv_T$ is valid, whereas, for the level l, it is not so. This may lead to a theoretical prediction of more sharp structures than those observed experimentally, because the contour at the level l can no longer be considered exponential. It represents a convolution of the Lorentzian and Gaussian profiles [13]. Thus, the dip, which is observed in this scheme instead of a peak will be blurred. In addition, the approximation $\Gamma_{nl} \ll \tau_D^{-1}$ is not fully satisfied in this scheme; therefore, coherent processes neglected in this theory can make an appreciable contribution to the shape of the tuning curve. All these factors may result in a difference between the theoretical and experimental curves, but the basic difference of this laser scheme from the previous one (the absence of a peak) must take place.

3. Experiment

A discharge tube of an argon laser was used as a cell with the Raman-laser active medium. The experiments were performed under conditions of a homogeneous discharge at a current of < 150 A in a sectioned discharge tube 7 mm in diameter and 0.5 m long with mirrors mounted in vacuum. Figure 2 shows a schematic of the experimental setup. The discharge tube (*1*) was placed inside the cavity with mirrors (*2*) and (*3*), which had a high reflectivity in the blue spectral region and were transparent in the red region. Thus, the pump and generated fields in the medium were represented by travelling and standing waves, respectively.

The Raman laser was pumped by tunable single-frequency cw dye lasers. Rhodamine 6G and DCM dyes were used in the dye laser for measurements in the schemes with long-lived and short-lived final levels, respectively. When the rhodamine 6G dye laser was used, the tuning was performed within a range of up to 20 GHz by heating a thick etalon and simultaneously tuning a thin etalon. In experiments with the DCM dye laser, the lasing power was continuously tuned within a range of up to 4.5 GHz [14] by the automatic control of the position of a Troitskii film. A short-term frequency stability was 10–20 MHz over the time interval of an order of 1s. The scheme shown in Fig. 2 corresponds to the setup with the DCM dye laser.

The beam from the dye laser (*4*) was focused by a lens (*5*) at the center of the discharge tube in order to ensure a maximum field homogeneity in the cavity. The pump field intensity inside the Raman laser cavity was ~ 1 W cm^{-2}. The frequency of the dye laser was measured by a wavelength meter (*6*) with a 100-MHz resolution. The Raman signal was selected with the help of a diffraction grating (*7*) and recorded with a photodetector (*9*). Scanning Fabry–Perot interferometers (*8*) with a 5-GHz free dispersion range were used to monitor the mode composition of the dye-laser radiation and Raman lasing.

Measurements were performed for various discharge currents, pressures, and pump powers. In all the measurements, the pump power corresponded to the linear absorption regime. In addition to the tuning curves of the Raman laser, linear absorption contours in the absence of lasing in the cell were recorded for all current values. The population of the level n, Doppler width kv_T, and the optical width αL were calculated from these profiles.

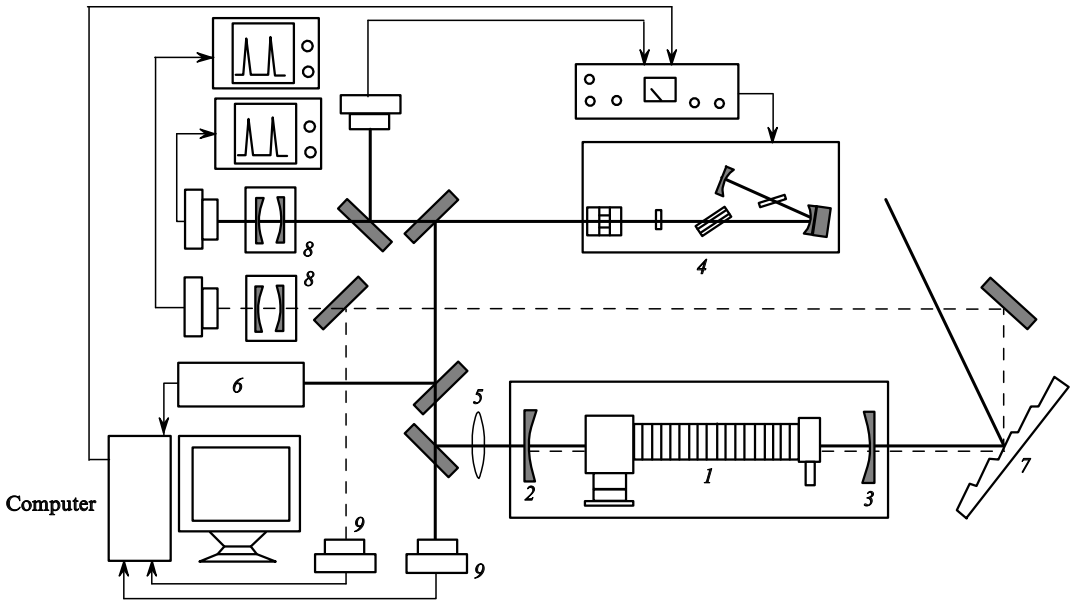

Figure 2. Schematic of the experimental setup: (*1*) discharge tube; (*2*, *3*) mirrors; (*4*) dye laser; (*5*) lens; (*6*) wavelength meter; (*7*) diffration grating; (*8*) scanning Fabry–Perot interferometers; and (*9*) photodiodes.

Figure 3 shows an experimental dependence of the Raman-laser output power on the pump frequency in the scheme with a long-lived final level [12], which was obtained under conditions when the approximations adopted in the theory considered above were valid. This figure also presents a curve calculated using formula (1). The curve was fitted by varying the parameter $q = (\Gamma_m/\Gamma_l)^{1/2}$ and the scaling factor C. The parameters P/τ and N/τ were estimated from independent measurements. The data were processed using the following values of parameters: $\nu = 2D/v_T^2 = 0.1\Gamma_m$, $N/\tau = 0.53$, $P/\tau = 6.8$, $kv_T = 3.2$ GHz, $\alpha L = 1.5$, and $A = 0.5q^2$, which corresponded to the experimental conditions. The central parts of the contours ($|\Omega_p| < k_p v_T$) were fitted, because the approximations of the theory are violated at their wings.

The obtained value of $q \simeq 1.3$ makes it possible to evaluate $\Gamma_m/\Gamma_l \simeq 1.7$, which agrees with the data reported in [8, 9]. The peak width is determined by the velocity diffusion at the level m: $\Delta_{D_m} = kv_T(\nu/2\Gamma_m)^{1/2} = 0.7$ GHz. We should take into account that the peak in the tuning curve is half as wide as the Bennett peak in the distribution over velocities. Figure 3 also shows that the peak amplitude is somewhat higher than that predicted theoretically. A probable explanation of this fact is a saturation with respect to the pump field neglected by the theory.

When $|\Omega_p| > k_p v_T$, the contribution of two-photon effects rises and may lead to an appreciable changes in the wings of the tuning curve. The absolute peak height (the pedestal is subtracted) increases linearly with the pump power P. This points to the predominance of the second term in formula (1), which is proportional to the power P, and indicates that the absorption saturation [15] is negligibly small under the experimental conditions.

Figure 4 presents the radiation power generated by the Raman laser as a function of the pump wave frequency for the scheme with the $4s\,^2P_{1/2}$ short-lived final level (Fig. 1b)

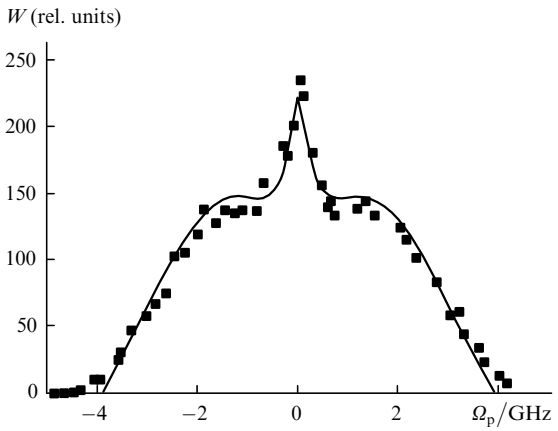

Figure 3. Lasing power W of a Raman ion laser versus detuning Ω_p of the exciting field in the scheme with a long-lived final level: (solid line) theoretical curve at $q = 1.3$ and (dots) experimental points.

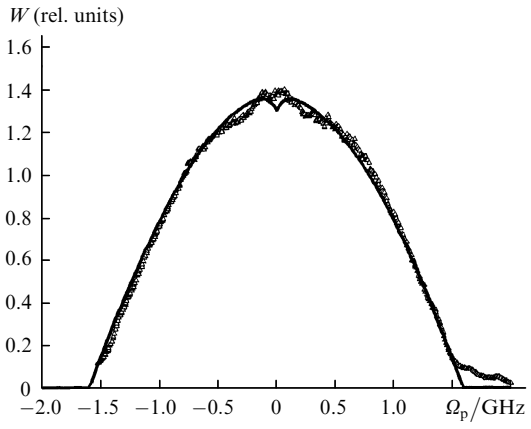

Figure 4. Lasing power W of a Raman ion laser versus detuning Ω_p of the exciting field in the scheme with a short-lived final level: (solid line) theoretical curve at $q = 0.2$ and (dots) experimental points.

and a fitting curve with the parameters $P/\tau = 0.45$ and $N/\tau = 0.99$ [see (1)]. The data were processed using the following parameters: $q = 0.2$, $\nu = 0.1\Gamma_m$, $kv_T = 3.2$ GHz, $\alpha L = 1.5$ and $A = 0.7q^2$, which correspond to the experimental conditions. The values of P/τ and N/τ resulting from this fitting agree with the estimates obtained from independent measurements.

Figure 4 shows that, in contrast to the scheme with a long-lived final level, a sharp peak is absent, as predicted by the theory. A change in the pump power resulted only in a change in its excess over the threshold and, thus, in a scaling of the entire tuning-curve contour as a whole. A shallow dip is observed at the contour centre, but its amplitude is comparable to the measurement error. Moreover, there is a slight elevation ~ 0.5 GHz wide at its centre with the dip at its top. This structure is probably a result of the influence of a coherence at the forbidden transition, which, as was shown above, may manifest itself in this scheme.

Measurements in the scheme with a short-lived final level were also performed at various pressures and discharge currents. However, the resulting dependences are not illustrative and are related only to a change in the inversion N from negative (absorption) to positive (amplification) values with the increasing current and decreasing pressure. This resulted in an increase in the contour amplitude and width without a significant change in its shape.

4. Conclusions

Plasma features of the active medium determine the tuning curves of a Raman ion laser with a travelling pump wave and a standing generated wave. Unlike neutral gases, in the case of the scheme with a long-lived final level, a comparatively wide peak is observed instead of a narrow two-photon dip. The peak shape is determined by the Coulomb broadening of the Bennett structure induced by the optical pumping at the intermediate level. The peak width is ~ 700 MHz, which is an order of magnitude larger than the width of the forbidden transition and is much smaller than the Coulomb width at the lower level. In the scheme with a short-lived final level, the peak is not observed, because the resonance structures induced by the optical pumping and saturation have close widths. The Raman laser theory [12] describes well the phenomenon under study in the first and second schemes.

The main mechanism in the formation of spectral structures near the resonance is an effect associated with the optical pumping combined with the saturation at various diffusion widths of the Bennett structures at the operating levels. Specific features of an ion Raman laser are determined by Coulomb collisions, which have a stronger broadening effect on the Bennett structures at levels with longer lifetimes.

Acknowledgements. The authors thank E.V. Podivilov, M.G. Stepanov, and D.A. Shapiro for useful discussion of the results of this study. This work was supported in part by the Russian Foundation for Basic Research (Grant Nos 00-15-96808 and 01-02-06422).

References

1. Agrawal G.P. *Nonlinear Fiber Optics* (New York: Academic Press, 2001).
2. Feitisch A., Schnier D., Müller T., Wellegehausen B. *IEEE J. Quantum Electron.*, **24**, 507 (1988).
3. Apolonsky A.A., Babin S.A., Chernykh A.I., Kablukov S.I., Khorev S.V., Podivilov E.V., Shapiro D.A. *Phys. Rev. A*, **55**, 661 (1997).
4. Beterov I.M., Matyugin Yu.A., Chebotaev V.P. *Opt. Spektrosk.*, **28**, 357 (1970).
5. Baklanov E.V., Beterov I.M., Dubetskii B.Ya., Chebotaev V.I *Pis'ma Zh. Eksp. Teor. Fiz.*, **22**, 289 (1975).
6. Rittner K., Höpe A., Müller-Wirts T., Wellegehausen B. *IEEE J. Quantum. Electron.*, **28**, 342 (1992).
7. Rittner K., Wicht A., Jordan G., Heuer A., Welling H., Wellegehausen B. *Laser Phys.*, **4**, 339 (1994).
8. Luyken B.F.J. *Phys.*, **60**, 432 (1972).
9. Hibbert A., Hansen J.E. *J. Phys. B: At. Mol. Opt. Phys.*, **27**, 3325 (1994).
10. Babin S.A., Kablukov S.I., Kobtsev S.M. *Opt. Spektrosk.*, **84**, 915 (1998).
11. Babin S.A., Shapiro D.A. *Phys. Rep.*, **241**, 119 (1994).
12. Babin S.A., Kablukov S.I., Khorev S.V., Podivilov E.V., Potapov V.V., Stepanov M.G., Shapiro D.A. *Phys. Rev. A*, **63**, 1 (2001).
13. Smirnov G.I., Shapiro D.A. *Zh. Eksp. Teor. Fiz.*, **76**, 2084 (1979).
14. Kobtsev S.M., Korablev A.V., Kukarin S.V., Sorokin V.B. *Proc. SPIE Int. Soc. Opt. Eng.*, **4353**, 189 (2001).
15. Lisitsin V.N., Chebotaev V.P. *Zh. Eksp. Teor. Fiz.*, **54**, 419 (1968).